eTransportation 27 (2026) 100515

Contents lists available at ScienceDirect

eTransportation

journal homepage: www.journals.elsevier.com/etransportation

Multi-timescale electricity cost optimization for commercial buildings using EV second-life battery as energy storage systems

Zhi Cao, Naser Vosoughi Kurdkandi, Shengyu Jia, Chris Mi *

Department of Electrical and Computer Engineering, San Diego State University, 5500 Campanile Drive, San Diego, 92182, CA, USA

ARTICLE INFO

Keywords:
Multi-timescale optimization
Second-life battery
Model predictive control
Demand charge management
Commercial building
Energy storage

ABSTRACT

The rapid growth of electric vehicles creates significant opportunities for stationary energy storage through second-life battery utilization. This paper proposes a multi-timescale electricity cost optimization framework for second-life battery energy storage systems (SLBESS) in commercial buildings and validates it on a real deployed system. To address the complex challenge of commercial tariffs that include both energy and demand charges, our approach decomposes the problem by timescale. An upper layer uses hourly model predictive control (MPC) with a rolling horizon for long-term energy arbitrage, while a lower layer employs real-time control to mitigate short-term power peaks. Critically, the framework integrates empirically validated, health-preserving constraints for second-life batteries, including a restricted 15%–85% state-of-charge window and a 0.25 C-rate current limit, directly linking battery longevity to economic optimization. Comprehensive validation using 12 months of real-world operational data from a deployed SLBESS demonstrates a 28.6% electricity cost reduction compared to no-storage operation, outperforming baseline rule-based and Lyapunov optimization methods by 6% and 16.1%, respectively. The framework ensures sub-500 ms computation times, achieves a modest annual battery degradation rate of 1.20%, and delivers a 5.0-year payback period, highlighting its practical viability and performance in real-world commercial applications.

1. Introduction

The rapid adoption of electric vehicles (EVs) is creating new opportunities for stationary energy storage through second-life battery utilization [1]. When EV batteries reach 70%–80% of their original capacity, they remain viable for less demanding stationary energy storage applications, offering significant cost advantages over new battery systems [2]. For commercial buildings with photovoltaic (PV) generation, second-life battery energy storage systems (SLBESS) present an attractive solution for electricity cost reduction through strategic energy management.

In many regions, commercial electricity pricing is based on time-of-use (TOU) tariffs that include both energy and demand charges. Energy charges are calculated based on total electricity consumption during a certain period of time during a day, while demand charges are based on peak power draw during the billing cycle. This dual pricing structure creates complex optimization problems that span different timescales: energy charges require long-term planning, while demand charges are sensitive to short-term peaks. Designing a control strategy that addresses both objectives efficiently is a major challenge.

Significant research efforts have been devoted to energy storage optimization considering both energy and demand charges. Traditional control approaches have relied on rule-based methods that implement simple heuristics such as charging during off-peak hours and discharging during peak periods [3]. While straightforward to implement, these methods lack optimality guarantees and fail to adapt to dynamic pricing and load conditions. Lyapunov optimization provides theoretical stability guarantees for online energy management [4], but the critical trade-off parameter between battery preservation and instantaneous cost is difficult to tune in practice, often yielding conservative performance. Dynamic programming (DP) approaches [5] can handle demand charge optimization but suffer from computational complexity. Data-driven approaches like deep reinforcement learning (DRL) [6,7] do not rely on *a priori* information but these methods require extensive training data and lack interpretability, making them challenging for practical deployment.

Model predictive control (MPC) is widely used in energy systems because it handles constraints and forecasts naturally [8–10]. However, applying MPC to energy and demand charge optimization presents significant computational challenges. Centralized approaches that simultaneously optimize both energy and demand charges result in prohibitively large optimization problems. Hasan et al. [11] demonstrated that day-ahead optimization with 15-minute resolution for demand

* Corresponding author.
E-mail address: cmi@sdsu.edu (C. Mi).

https://doi.org/10.1016/j.etran.2025.100515
Received 4 August 2025; Received in revised form 17 November 2025; Accepted 18 November 2025
Available online 24 November 2025

Table 1
Advanced techniques of BESS cost optimization.

Reference	Method	Achievements	Limitations
[16]	Multi-agent RL	14.68% cost reduction vs. no BESS; 3.56% more savings than DRL baselines	Training complexity and hyper-parameter sensitivity
[17]	Hierarchical multi-agent RL	29.5% total cost reduction vs. baseline; balances cost and comfort	Validated on residential scale only
[18]	Dynamic programming	62 s computation time; 33.6–94.8% operational cost savings across scenarios	Savings highly scenario-dependent; requires accurate forecasts and degradation model
[19]	Deep learning + optimization	Day-ahead scheduling with demand charge consideration; reduces daily electricity cost in realistic case studies	Residential focus; performance hinges on forecast accuracy
[20]	Genetic algorithm + rule-based	Energy consumption decreases 19%–21%, peak demand decreases 33%–50%;	Focuses on peak shaving more than full bill minimization; depends on prediction quality

charge management generates 96 time steps, with the number of decision variables growing rapidly, making the problem computationally intensive for real-time implementation. Furthermore, day-ahead prediction of load and solar generation at 15-minute resolution is prone to significant forecast errors due to high uncertainty at fine temporal resolutions. Multi-timescale control strategies have been explored in microgrids and thermal systems [12–14], and some have been applied to BESS at the distribution level [15]. However, their use in commercial buildings with both energy charge and demand charge objectives remains largely unexplored.

Table 1 summarizes recent advanced techniques for battery energy storage system (BESS) optimization, highlighting diverse approaches with varying strengths and limitations. While these approaches demonstrate notable cost savings and peak demand reductions, two critical gaps remain. First, joint optimization of energy and demand charges often results in computationally intensive formulations that are unsuitable for real-time implementation. Although reinforcement learning (RL) frameworks help mitigate this complexity, they introduce new challenges, including long training periods, high data requirements, and limited interpretability. Second, most existing studies are validated solely through simulation, with limited evidence from real-world deployments under commercial tariff structures. These limitations underscore the need for a framework that is both computationally tractable and empirically validated.

This paper addresses these gaps by proposing a hierarchical multi-timescale control framework for SLBESS in commercial buildings. The key contributions are:

(1) A tailored temporal decomposition for commercial tariffs: The framework explicitly decouples the optimization of cumulative energy charges (managed by an hourly MPC) from the mitigation of non-convex demand charges based on 15-minute peaks (managed by a real-time greedy algorithm). This provides a computationally efficient solution to a problem where centralized approaches are often intractable.
(2) Validation with real-world deployment: The proposed method is validated on a real SLBESS, demonstrating its practical performance and robustness under realistic conditions of forecast uncertainty and system constraints.

The proposed framework is validated using 12 months of operational data. The results demonstrate a 28.6% cost reduction, 1.20% annual battery degradation, and a 5-year payback period, supporting its practical value for commercial applications.

The remainder of this paper is organized as follows: Section 2 presents the system model and problem formulation, Section 3 describes the hierarchical control framework, Section 4 presents experimental results, and Section 5 concludes the paper.

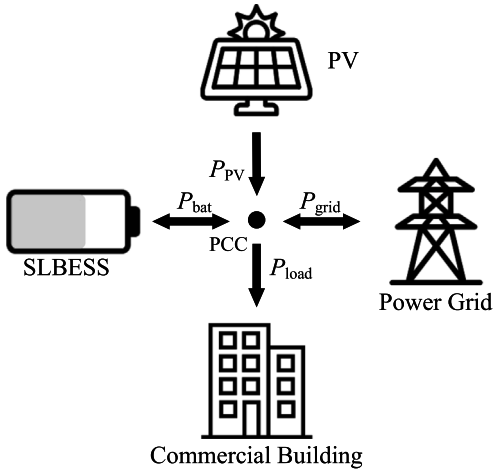

Fig. 1. System architecture diagram.

2. System model and problem formulation

This section establishes the mathematical foundation for the multi-timescale electricity cost optimization problem, encompassing the commercial building microgrid architecture and energy flows, the dual-component electricity pricing structure, and the system dynamics and operational constraints of second-life battery energy storage systems. The complete optimization problem is then formulated, highlighting the computational challenges that motivate the hierarchical decomposition approach developed in Section 3.

2.1. System description

Fig. 1 illustrates the system architecture of a typical commercial building with SLBESS integration. The microgrid includes a point of common coupling (PCC) to the utility grid, a photovoltaic (PV) system, the SLBESS, and aggregate building loads. The battery system operates in grid-tied mode. The energy flows in the system follow these directions: bidirectional power exchange between the building and utility grid, bidirectional charging/discharging of the SLBESS, and the unidirectional PV generation to the building, grid, or battery storage.

2.2. Electricity cost structure

Commercial electricity pricing in many regions, including California, follows a TOU structure consisting of energy charges and demand charges. This dual-component pricing creates distinct optimization objectives that operate at different timescales.

The energy charge is based on total electricity consumption and varies by time period:

$$J_E = \Delta t \sum_{t=0}^{T-1} \left[c_{\text{imp}}(t) \max(P_{\text{grid}}(t), 0) + c_{\text{exp}}(t) \min(P_{\text{grid}}(t), 0) \right] \tag{1}$$

where Δt is the time interval, T is the total number of time steps in each billing cycle, $P_{\text{grid}}(t)$ is net grid power (positive for import, negative for export), $c_{\text{imp}}(t)$ is the import electricity price ($/kWh), and $c_{\text{exp}}(t)$ is the export price ($/kWh). The formulation ensures that energy charges are calculated separately for import and export, accounting for different pricing structures.

The demand charge is based on the peak 15-minute average power import during the entire billing cycle:

$$J_D = c_d(t^*) \cdot \max_{t \in \mathcal{T}} P_{\text{imp}}(t) \tag{2}$$

where $c_d(t^*)$ is the demand charge rate ($/kW) corresponding to time t^* when peak grid import occurs, $\mathcal{T}$ represents all 15-minute time windows within the billing period, and $P_{\text{imp}}(t) = \max(P_{\text{grid}}(t), 0)$ is the grid import power averaged over 15-minute windows. This formulation captures the time-dependent nature of demand charges, which often vary between on-peak and off-peak periods. The TOU rates for energy charge and demand charge used in this paper are given in Section 4.1.

The total electricity cost combines both components:

$$J_{\text{total}} = J_E + J_D \tag{3}$$

The key insight for the multi-timescale approach is that energy charges accumulate over hours and benefit from long-term optimization based on TOU pricing patterns, while demand charges depend on instantaneous power peaks and require fast response capability to avoid peak coincidence.

2.3. System dynamics and constraints

This paper considers discrete-time modeling of the system. The power balance at the PCC follows:

$$P_{\text{grid}}(t) = P_{\text{load}}(t) - P_{\text{PV}}(t) + P_{\text{bat}}(t) \tag{4}$$

where $P_{\text{load}}(t)$, $P_{\text{PV}}(t)$, and $P_{\text{bat}}(t)$ represent building load, PV generation, and net battery power (positive for charging, negative for discharging), respectively.

To facilitate linear optimization and explicitly handle battery efficiency and operational constraints, the battery power $P_{\text{bat}}(t)$ is decomposed into two non-negative variables: the charging power $P_{\text{cha}}(t)$ and discharging power $P_{\text{dis}}(t)$. This leads to the formulation:

$$P_{\text{bat}}(t) = P_{\text{cha}}(t) - P_{\text{dis}}(t) \tag{5}$$

where at each time step, at most one of $P_{\text{cha}}(t)$ and $P_{\text{dis}}(t)$ is nonzero. Alternatively, in numerical implementations, this condition can be relaxed using binary variables in post-processing.

The battery state of charge (SOC) evolution follows:

$$SOC(t+1) = SOC(t) + \frac{\eta_{\text{cha}} P_{\text{cha}}(t) - P_{\text{dis}}(t)/\eta_{\text{dis}}}{E_{\max}} \cdot \Delta t \tag{6}$$

where η_{cha} and η_{dis} are charging and discharging efficiencies, $E_{\max}$ is the full battery capacity.

The battery operates under conservative constraints that preserve longevity for second-life applications:

$$0 \le P_{\text{cha}}(t) \le P_{\text{bat,cha}}^{\max} \tag{7}$$

$$0 \le P_{\text{dis}}(t) \le P_{\text{bat,dis}}^{\max} \tag{8}$$

$$SOC_{\min} \le SOC(t) \le SOC_{\max} \tag{9}$$

where $P_{\text{bat,cha}}^{\max}$ and $P_{\text{bat,dis}}^{\max}$ are the maximum battery charging and discharging power ratings. For second-life batteries, conservative SOC limits are employed: $SOC_{\min} = 15\%$ and $SOC_{\max} = 85\%$, which helps maintain capacity and extend operational life while avoiding deep cycling that accelerates degradation [21]. This approach is also supported by the lifespan study of first-generation Nissan Leaf packs in SLBESS applications [22].

Additionally, the system respects grid connection limits:

$$|P_{\text{grid}}(t)| \le P_{\text{grid}}^{\max} \tag{10}$$

where $P_{\text{grid}}^{\max}$ is the maximum allowed grid power exchange capacity.

2.4. Optimization problem formulation

The complete optimization problem seeks to minimize total electricity cost over a billing cycle:

$$\min_{\{P_{\text{bat}}(t)\}_{t=0}^{T-1}} \quad J_{\text{total}} = J_E + J_D \tag{11}$$

subject to constraints (4)–(10).

The coupling between energy and demand objectives across different timescales requires fine temporal resolution for demand management while maintaining long-term planning for energy arbitrage, creating computational complexity that grows with the time horizon. Besides, the stochastic nature of load and PV generation necessitates robust optimization strategies that can handle forecast uncertainties. Therefore, this formulation motivates the decomposition into computationally tractable sub-problems through a multi-timescale framework.

3. Multi-timescale framework

This section presents the proposed hierarchical energy management architecture that decomposes the complex electricity cost optimization into coordinated upper and lower control loops operating at different timescales.

3.1. Framework architecture

The multi-timescale framework, illustrated in Fig. 2, consists of two hierarchical control layers that exploit the natural temporal separation in commercial electricity pricing:

(1) Upper layer: optimizes energy arbitrage over a 24-hour rolling horizon with hourly resolution, focusing on minimizing energy charges through strategic charge/discharge scheduling based on TOU pricing.
(2) Lower layer: tracks upper-layer energy references while managing demand charges through real-time power flow control with minute-level resolution to avoid demand charge penalties.

The key advantage of this decomposition is the dramatic reduction in computational complexity while maintaining near-optimal performance. Instead of solving a single large optimization problem with 96 time steps for 24-hour optimization at 15-minute resolution, the framework solves a 24-time-step hourly problem and implements simple minute-level control rules.

3.2. Upper layer: Hourly energy arbitrage MPC

The upper layer optimizes energy charges by solving a 24-hour rolling horizon MPC problem updated every hour. This layer exploits TOU pricing differentials to maximize economic benefits through strategic energy arbitrage. Hourly prediction of load and solar generation is more computationally feasible compared to fine temporal resolutions.

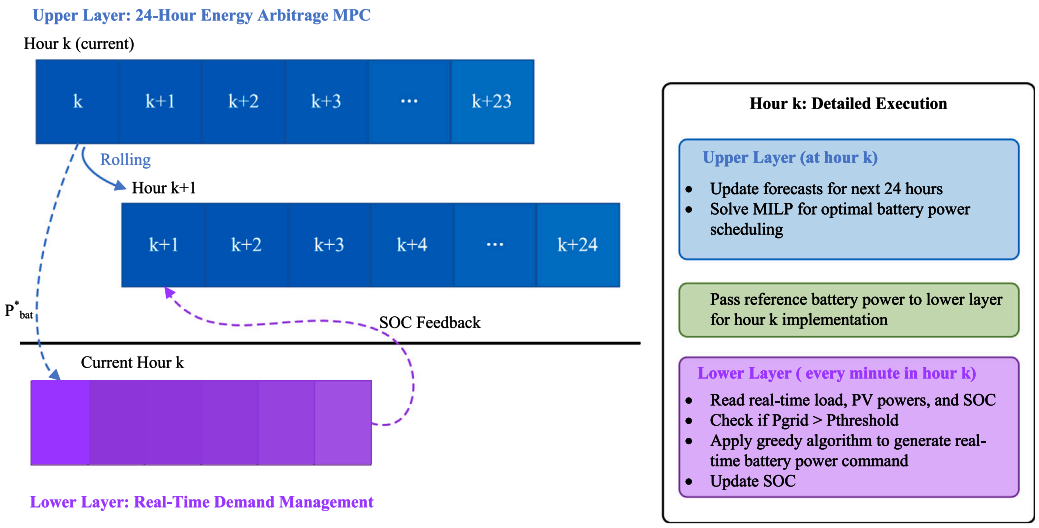

Fig. 2. Multi-timescale energy management architecture.

3.2.1. MILP problem formulation

To ensure computational tractability and global optimality, the energy charge optimization is formulated as a mixed-integer linear programming (MILP) problem. MILP is well-established for energy system optimization. The energy charge is reformulated with separate variables for grid import power P^h_{imp} and grid export power P^h_{exp} to eliminate nonlinear max/min operations [23]:

$$J_E = \sum_{h=k}^{k+23} \left[c_{\text{imp}}(h) P^h_{\text{imp}} - c_{\text{exp}}(h) P^h_{\text{exp}} \right] \cdot \Delta h \tag{12}$$

where the superscript h in this subsection denotes hourly-scale variables, and $\Delta h = 1$.

Complementary constraints using binary variables enforce mutually exclusive import/export operations, which is essential for accurate cost calculation under different import and export pricing [15]:

$$0 \le P^h_{\text{imp}} \le g^h \cdot P^{\max}_{\text{grid}} \tag{13}$$

$$0 \le P^h_{\text{exp}} \le (1 - g^h) \cdot P^{\max}_{\text{grid}} \tag{14}$$

where $g^h \in \{0, 1\}$ is the binary variable (1 for import, 0 for export).

Similarly, battery charging and discharging should be mutually exclusive to avoid simultaneous charging and discharging:

$$0 \le P^h_{\text{cha}} \le z^h \cdot P^{\max}_{\text{bat,cha}} \tag{15}$$

$$0 \le P^h_{\text{dis}} \le (1 - z^h) \cdot P^{\max}_{\text{bat,dis}} \tag{16}$$

where $z^h \in \{0, 1\}$ is the binary variable (1 for charging, 0 for discharging).

The complete MILP formulation includes the following constraints:

$$P^h_{\text{imp}} - P^h_{\text{exp}} = P^h_{\text{load}} - P^h_{\text{PV}} + P^h_{\text{cha}} - P^h_{\text{dis}} \tag{17}$$

$$SOC^{h+1} = SOC^h + \frac{\eta_{\text{cha}} P^h_{\text{cha}} - P^h_{\text{dis}} / \eta_{\text{dis}}}{E_{\max}} \cdot \Delta h \tag{18}$$

$$SOC_{\min} \le SOC^h \le SOC_{\max} \tag{19}$$

$$SOC^k = SOC_{\text{current}} \tag{20}$$

where SOC_{current} is the actual battery state at the beginning of hour k, updated from the lower layer's real-time operation.

At each hour k, the upper layer solves the following optimization problem:

$$\min_{\substack{P^h_{\text{cha}}, P^h_{\text{dis}}, P^h_{\text{imp}}, P^h_{\text{exp}}, \\ z^h, g^h}} \sum_{h=k}^{k+23} \left[c_{\text{imp}}(h) P^h_{\text{imp}} - c_{\text{exp}}(h) P^h_{\text{exp}} \right] \cdot \Delta h \tag{21}$$

subject to constraints (13) to (20) over prediction horizon $h \in [k, k+23]$, corresponding to 24 hourly steps starting from hour k.

This MILP formulation of upper layer generates optimal hourly battery power references $P^{h,*}_{\text{bat}} = P^{h,*}_{\text{cha}} - P^{h,*}_{\text{dis}}$ for cost-optimal energy arbitrage.

3.2.2. Forecasting model

This paper employs eXtreme Gradient Boosting (XGBoost) regression models for load and PV prediction due to their superior performance in handling nonlinear patterns and temporal dependencies in energy systems [24,25]. XGBoost has demonstrated excellent performance in energy forecasting applications, particularly for capturing complex relationships between meteorological variables and energy consumption patterns.

The forecasting models use comprehensive feature sets derived from available data: historical data including load and PV values from past 48 h to capture daily and weekly patterns, temporal features such as the hour of day, day of week, month, and season to account for systematic variations, and binary indicators including weekend/weekday flags and holiday indicators to capture behavioral differences.

3.3. Lower layer: Real-time demand management

The lower layer operates every minute to track upper-layer references while managing demand charges through a computationally efficient greedy algorithm. Greedy algorithms are well-suited for real-time energy storage management when the optimization horizon is short and immediate response is critical [26]. The algorithm focuses on minimizing grid power import during 15-minute demand charge windows while maintaining coordination with the upper layer's energy arbitrage objectives.

The demand charge structure in Eq. (2) implies that the optimization objective is to minimize the maximum power import across all 15-minute windows in the billing cycle. Since demand charges are determined by peak power rather than cumulative energy, the optimization can be approached greedily by avoiding power peaks whenever possible, subject to battery and SOC constraints.

At each minute m within hour k, the lower layer determines battery power using the following decision rule:

$$P^{k,m}_{\text{bat}} = \begin{cases} P^{k,*}_{\text{bat}}, & \text{if } P^{k,m*}_{\text{grid}} \le P_{\text{threshold}} \\ \min(P^{k,*}_{\text{bat}} - (P^{k,m*}_{\text{grid}} - P_{\text{threshold}}), P^{\max}_{\text{bat}}), & \text{if } P^{k,m*}_{\text{grid}} > P_{\text{threshold}} \end{cases} \tag{22}$$

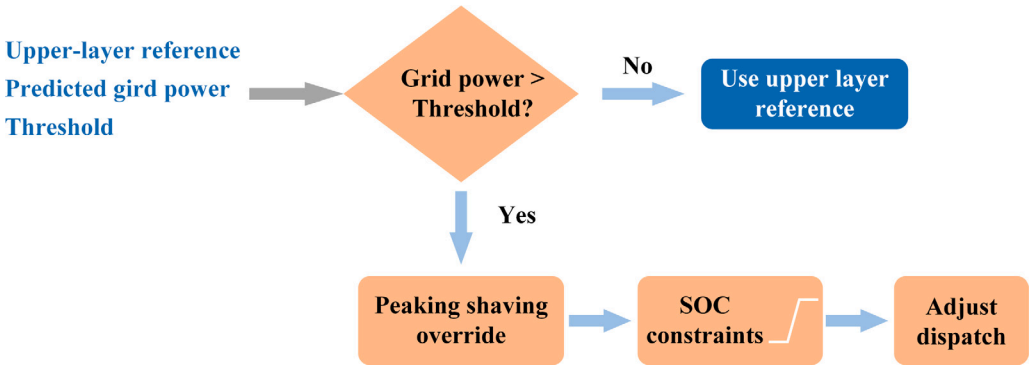

Fig. 3. Flowchart of lower layer greedy algorithm.

where $P_{\text{grid}}^{k,m*} = P_{\text{load}}^{k,m} - P_{\text{PV}}^{k,m} + P_{\text{bat}}^{k,*}$ is the predicted net grid power with the upper layer reference, and $P_{\text{threshold}}$ is the demand limit threshold. The complete lower layer algorithm is presented in Fig. 3. As shown, the algorithm evaluates whether the predicted grid power exceeds the demand threshold. If so, it applies peak shaving override per Eq. (22); otherwise, it tracks the upper-layer reference.

The threshold $P_{\text{threshold}}$ is a critical parameter that balances immediate demand charge avoidance with long-term energy arbitrage benefits. A lower threshold provides more aggressive demand management but may compromise energy arbitrage by frequently overriding upper layer references. A higher threshold preserves energy arbitrage strategies but may miss opportunities for demand charge reduction. The threshold selection and its impact on system performance will be analyzed in the experimental results section.

3.4. Implementation algorithm

The coordination between upper and lower layers ensures system-wide performance through reference passing (upper layer provides hourly battery power references), state feedback (actual SOC from lower layer updates upper layer initialization), priority management (lower layer prioritizes demand management when grid power exceeds threshold), and constraint consistency (both layers enforce identical battery and SOC constraints). The complete implementation procedure of the proposed method is summarized in Algorithm 1 (see Appendix). The hierarchical loop forms a feedback control system: the actual battery SOC is continuously updated to the upper layer, ensuring consistency between planned and executed trajectories.

3.5. Remarks

The proposed hierarchical control framework balances optimality and computational efficiency through a natural temporal decomposition. The upper layer MILP formulation guarantees optimality within each 24-hour prediction horizon under perfect forecasts due to its linear objective and convex constraints. The lower-layer greedy algorithm executes minute-level demand management by overriding upper-layer references only when grid import exceeds a predefined threshold. Although this strategy may occasionally cause deviation from the upper-layer plan, it ensures compliance with demand charge objectives while respecting battery constraints. The lower layer greedy algorithm is computationally efficient since only algebraic threshold checks and saturation logic are involved. While the coordination between layers introduces some sub-optimality compared to centralized approaches, this trade-off enables computational tractability while maintaining reasonable performance, justified by the natural temporal separation between cumulative energy charges and instantaneous demand charges.

4. Experimental results and analysis

This section presents comprehensive validation of the proposed multi-timescale framework using real operational data from a deployed SLBESS system. The validation approach combines numerical simulation with field data to ensure both accuracy and comprehensive comparison.

The performance comparison of the three control strategies (rule-based, Lyapunov optimization, and the proposed method) is conducted through numerical simulation using real load and PV generation data from an operational SLBESS deployment. This simulation-based approach is necessary because implementing multiple control strategies simultaneously on the same physical system for comparison is impractical and potentially unsafe. To ensure simulation accuracy, we validate the proposed method by comparing its simulation results with actual field operation data, demonstrating excellent agreement between simulated and real performance.

4.1. Experimental setup

Fig. 4 demonstrates the second-life battery system used in this paper for validation. It is deployed at a warehouse at 7835 Trade Street, San Diego, CA, which is a surplus management facility operating Monday–Friday, 10:00 AM–5:00 PM. The load factor of this building is 0.33 and the capacity of the PV system is 200 kW.

The experimental platform integrates six retired EV battery packs with commercial power conversion equipment and custom control systems. The system architecture follows a hierarchical design where battery packs connect to a common DC bus via bidirectional DC–DC converters, while a three-phase inverter links the DC bus to the PCC. One battery pack is directly connected to the DC bus, serving as a buffer. This configuration primarily stabilizes the DC-link voltage and mitigates in-rush currents and voltage spikes during converter and inverter switching, thereby improving system reliability. This design was adopted after initial deployment revealed that the commercial DC–DC converters in this project were particularly vulnerable to damage from these transients. The directly connected battery pack provides a robust, passive solution to protect this critical hardware. In this setup, the buffer pack operates as a passive element on the DC bus, while the remaining packs are actively controlled. The charge and discharge currents are controlled by the DC–DC converters, and the inverter works in the DC bus supply mode. This configuration results in distinct operational profiles, causing uneven aging across the battery packs. The buffer pack undergoes frequent, shallow cycles from system transients, while the controlled packs perform deeper, scheduled cycles for energy arbitrage and peak shaving. The annual degradation rate reported in this paper applies only to the actively cycled packs; the buffer pack, monitored separately, is excluded from this analysis. The descriptions of major system components are summarized in Table 2.

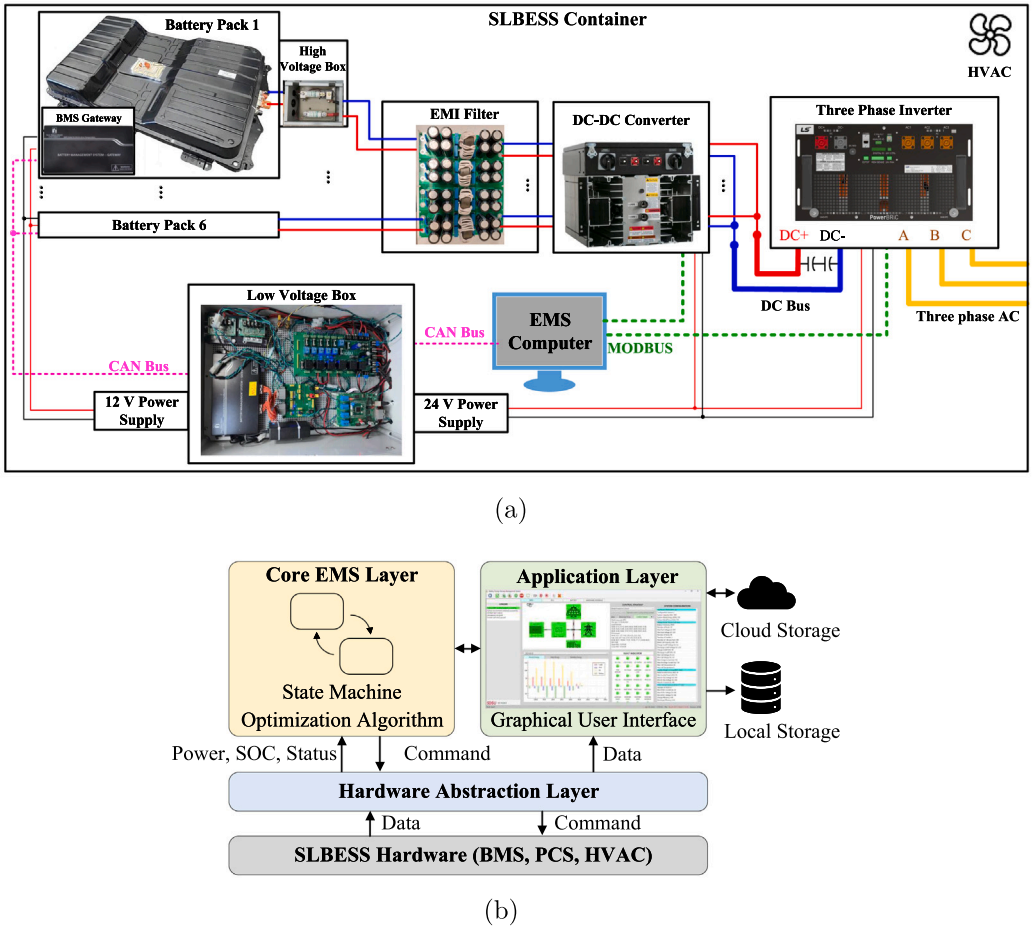

Fig. 4. Schematic diagram of test site. (a) SLBESS hardware connection diagram. (b) EMS function diagram.

The proposed control strategy is integrated into the energy management software (EMS) as shown in Fig. 4(b) for this battery system. The EMS software is developed in C++/Qt framework and operates on a dedicated industrial computer. The system architecture comprises three layers: (1) Hardware Abstraction Layer (HAL) interfacing with SLBESS components via Modbus and CAN protocols; (2) Core EMS Layer implementing the optimization algorithms and state machine control, (3) Application Layer providing graphical user interface for real-time monitoring, parameter adjustment, and data management supporting both local storage and cloud connectivity for remote access and analytics. The EMS executes the proposed hierarchical control framework with 1-minute data acquisition, hourly MPC optimization, and real-time demand management while logging all operational parameters for performance validation.

The TOU energy charge rate and feed-in tariff used in this paper are displayed in Fig. 5. The demand charge rates are: 33.08 $/kW for off-peak hours in summer and winter, 84.51 $/kW for summer on-peak hours, and 71.40 $/kW for winter on-peak hours.

The XGBoost forecast model was trained on historical operational data from May 2022 to May 2024. Minute-level measurements were aggregated into hourly data matching the upper-layer MPC timescale requirements. Table 3 shows the forecast accuracy of the XGBoost model used in this paper. The forecasting model's accuracy is moderate. Load forecasts demonstrate superior accuracy because building demand follows recurring schedules and calendar effects. In contrast, PV forecasts are less accurate in this study because of the absence of exogenous weather inputs (e.g., irradiance, cloud cover, temperature); under rapidly changing weather conditions, these missing features drive most of the error. Integration of weather variables would be expected to reduce PV forecast error.

The proposed control method is compared with two baseline control strategies: rule-based control and Lyapunov optimization. The Lyapunov baseline follows the Ref. [4] with its trade-off parameter tuned to the best-performing value over the study dataset under the same SOC and power constraints. The data spans from May 2024 to May 2025 (12 months) with 1-minute resolution.

4.2. Simulation validation with experimental data

To ensure the reliability of simulation results, we conducted a validation study comparing the proposed method's simulation results with actual field operation data. The proposed algorithm was implemented on the real SLBESS system for a one-month period, and the operational results were compared with simulation using identical load, PV, and pricing data.

Fig. 6 shows daily operation profiles comparing simulation and field data for a representative week. The validation demonstrates good agreement between simulation and field operation.

Table 4 presents the comparison between simulation and field operation. Statistical correlation analysis in Table 5 further confirms simulation accuracy with high correlation coefficients and low error metrics. Notably, the SOC trajectories show a higher correlation than instantaneous battery power, due to the cumulative and smoother nature of SOC dynamics. The small discrepancies observed are primarily due to unmodeled system dynamics, communication latencies, and measurement noise. The validation here provides confidence in the following comparative analysis results.

Table 2
System major components.

Category	Model	Specifications/Function
Second-life EV battery packs	Nissan Leaf Gen 3	• 56 kWh/152 Ah per pack (90% SOH[a]) • 15%–85% SOC operating range • 98.5% round-trip energy efficiency • Max. 0.25 C current per pack
BMS gateways	Custom-designed BMS interface	• Access to onboard BMS data • High-resolution sensing • State estimation • Relay control • Protection
Battery high voltage box	Custom interface units	• 50 A DC fuses for overcurrent protection • Shunt resistors for pack current measurement • Voltage terminals for voltage sensing
EMI filter	Custom-designed	• Electromagnetic interference mitigation
DC–DC converters	Alencon BOSS-1000	• 200–1000 V voltage range • Max. 19.2 kW per channel • 98.5% peak efficiency • Bidirectional power flow control for individual battery packs with galvanic isolation
Inverters	LS Energy Solutions PowerBRiC Gen2	• 56 kW AC • 208 V/60 Hz 3-phase AC output • 380 V DC bus • Unity power factor mode
Low voltage control box	Custom control module	• 12 V/24 V regulated supplies • CAN/Modbus routing • Relay control logic
Central control computer	Desktop workstation	Real-time system control running EMS software

[a] State of health (SOH) is defined as the ratio of measured usable capacity to the nominal capacity of the new pack. Capacity was tested through a standardized 0.2C (25 °C) constant current discharge testing.

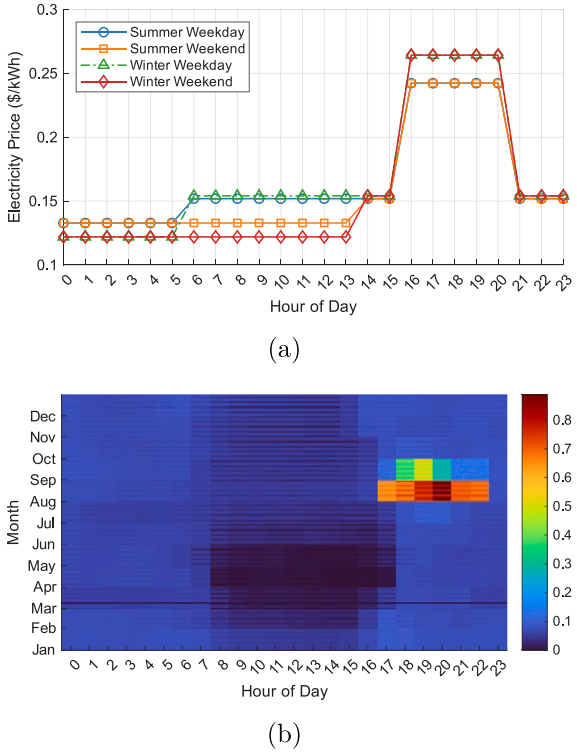

Fig. 5. TOU energy charge rate. (a) Buy price. (b) Sell price heatmap. (Summer: June to September. Winter: October to May).

The field validation reported herein covers a one-month window. While it shows good agreement between simulation and field operation for these periods, building load and PV generation can exhibit seasonal variability. Future work will extend field validation to cover complete annual cycles to capture long-term seasonal variations and battery aging effects.

Table 3
XGBoost forecasting performance metrics.

Variable	RMSE (kW)	MAE (kW)	R^2
Load	7.2	4.8	0.91
PV Generation	19.3	9.2	0.92

Table 4
Simulation vs. field operation validation.

Metric	Field data	Simulation	Error (%)
Grid Import Energy (kWh)	9162	9603	4.80
Grid Export Energy (kWh)	8492	8020	5.56
Grid Peak Power (kW)	97.1	94.9	2.29
Battery Energy Throughput (kWh/day)	820	821	0.12
Average SOC (%)	55.86	56.95	0.15
Total Cost ($)	5855	6088	3.98

Table 5
Statistical correlation analysis between simulation and field data.

Variable	Correlation (R^2)	RMSE	MAE
Battery Power	0.92	11.9 kW	7.6 kW
SOC Trajectory	0.97	4.6%	3.4%

4.3. Economic performance comparison

Table 6 summarizes the annual cost breakdown and savings for each control strategy. The proposed method achieves 28.6% cost reduction, significantly outperforming Lyapunov optimization (12.5%) and exceeding rule-based control (22.6%). The performance gap with perfect foresight is only 2.5%. The proposed multi-timescale MPC can effectively manage both energy and demand charges, achieving the highest cost reduction among practical algorithms.

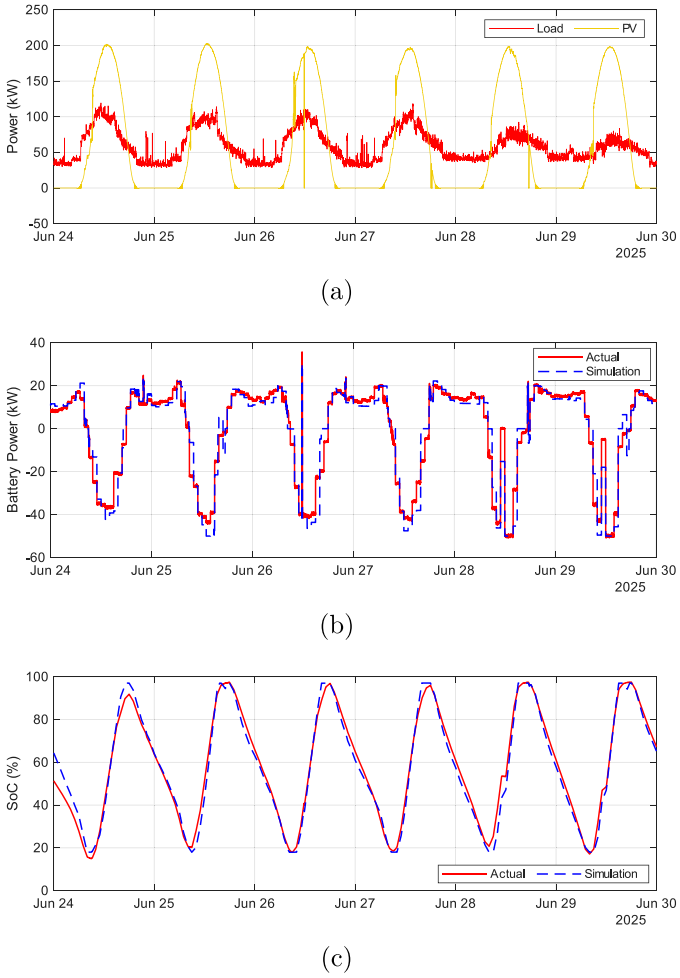

Fig. 6. Simulation and filed data comparison. (a) PV and load profiles. (b) Battery power. (d) SOC trajectories.

Table 6
Economic performance comparison.

Method	Total cost ($)	Energy charge ($)	Demand charge ($)	Savings (%)
No Storage	72 282	31 030	41 252	–
Rule-Based	55 928	20 872	35 056	22.6
Lyapunov	63 281	21 932	41 349	12.5
Proposed	51 606	19 396	32 210	28.6
Perfect Foresight	49 789	18 096	31 693	31.1

Table 7
Operational performance metrics.

Metric	Rule-based	Lyapunov	Proposed
Daily Throughput (kWh)	617	385	476
Equivalent Full Cycles /Year	311	194	240
Average SOC (%)	49.1	49.0	37.6
SOC Standard Deviation (%)	25.6	19.7	20.0
Average Charging Power (kW)	39.7	45.9	25.3
Average Discharging Power (kW)	31.9	40.4	23.2
Average Power Change Rate (kW/min)	1.6	4.7	0.4
Battery Utilization Rate (%)	70	37	70
Rainflow Cycle Count[a]	585	355	554
Average Cycle Depth (%)	51	47	43
Estimated Annual Degradation[b] (%)	1.56	0.97	1.20

[a] Rainflow cycle counting algorithm identifies complete charge–discharge cycles from SOC time series data following ASTM E1049 standard [27,28].

[b] Annual degradation estimated based on 5%/1000 equivalent full cycles (EFC) degradation rate for second-life batteries. This rate was empirically validated through comprehensive aging tests on identical second-life EV batteries under controlled conditions: 0.3C charge/discharge rate, 80% depth of discharge, and temperature below 30 °C [21]. The current system operates within these validated parameters.

4.4. Operational performance and battery health analysis

This section compares operational performance of the three control methods and analyzes their impact on battery health. Table 7 details operational characteristics and Fig. 7 shows the monthly trends of operational performance across the 12-month study period.

Rule-based control consistently delivers the highest daily energy throughput and capacity utilization, driven by its simple, reactive rules that aggressively dispatch energy whenever PV exceeds load or load exceeds PV. As shown in Fig. 7(a), its throughput increases during summer months when both PV generation and loads are high. The battery utilization time remains steady year-round, reflecting consistent responsiveness to PV-load imbalance. Both average charging and discharging power stay relatively stable, with a notable summer increase in discharging power. While simple to implement, this strategy induces the most aggressive cycling behavior, with the highest cycle count per year and the deepest average cycle depth. SOC profiles show wide fluctuations and high standard deviation, reflecting the reactive dispatch logic. The high-stress usage pattern leads to the highest estimated degradation rate of 1.56% annually.

Lyapunov optimization shows the lowest throughput and utilization time, particularly during summer months. This counterintuitive pattern

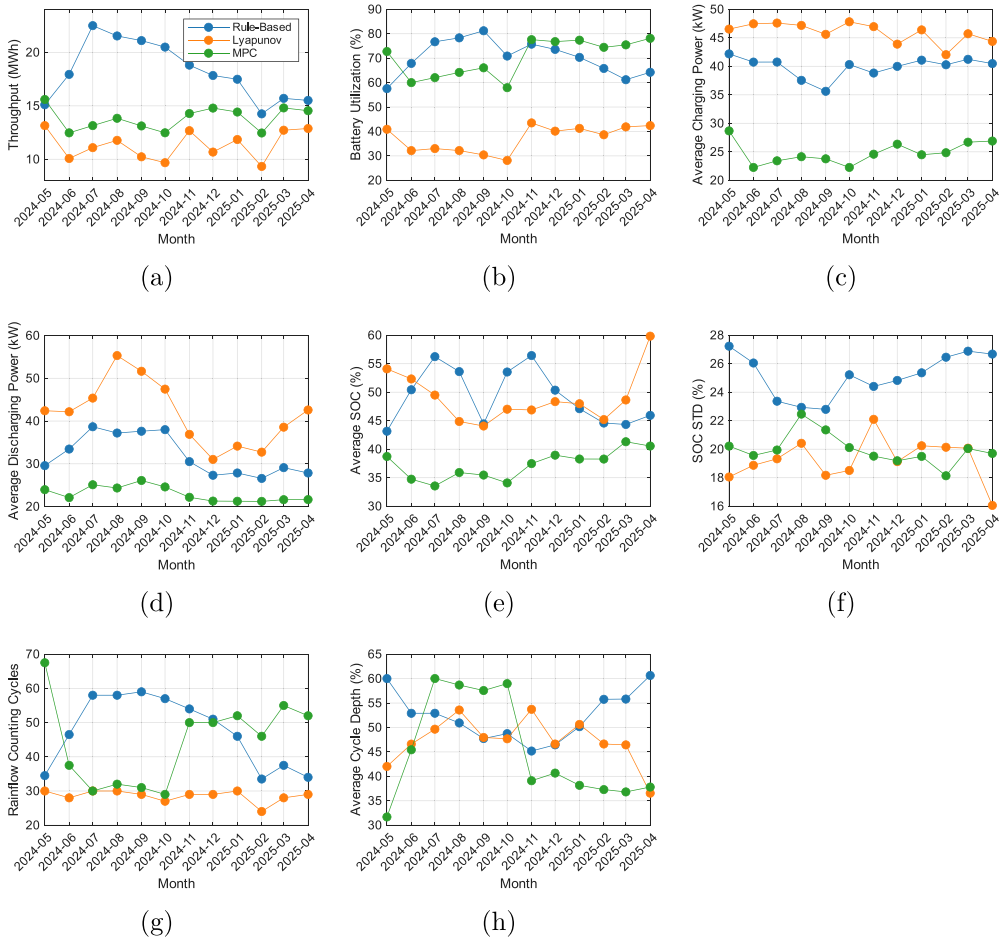

Fig. 7. Monthly operational performance: (a) Monthly throughput. (b) Battery utilization time. (c) Average charging power. (d) Average discharging power. (e) Average SOC. (f) SOC standard deviation. (g) Rainflow counting cycles. (h) Rainflow counting cycle depth.

arises from its cost-driven logic-higher electricity prices in winter increase dispatch activity, while summer PV abundance coincides with lower marginal savings from storage operation. Although charging and discharging powers remain high, Lyapunov optimization introduces frequent small-scale actions, resulting in the highest power change rate. Battery usage is sparse and conservative, with only 37% utilization rate and the lowest cycle count. The conservative operation results in the lowest estimated degradation rate, reflecting a trade-off between operational intensity and battery preservation.

The proposed method achieves a well-balanced performance profile with moderate throughput and stable battery utilization. The multi-timescale forecasting enables sustained, consistent low-power operation that avoids excessive cycling. The average SOC is well-centered with low standard deviation, indicating stable operation. The method achieves moderate degradation rate (1.20% annually), confirming stress-aware, health-preserving control behavior while maintaining high utilization efficiency. The approach successfully balances energy throughput with battery longevity, making it ideal for commercial second-life battery applications.

The substantial performance advantage over Lyapunov optimization reflects fundamental differences in algorithmic design. Lyapunov optimization minimizes a time-average proxy through myopic reactions to instantaneous states, while commercial demand charges penalize the maximum 15-minute import in a billing cycle. The proposed framework directly targets this peak objective through explicit demand-limit thresholding. Additionally, Lyapunov optimization operates reactively without forecast information, missing optimal TOU arbitrage opportunities that the proposed 24-hour MPC captures. The operational data reveals Lyapunov's suboptimal behavior: low utilization combined with the highest power change rate, indicating frequent small corrective actions that neither effectively shave peaks nor maximize energy arbitrage benefits.

Table 8 presents grid integration metrics of three control strategies. All three control strategies significantly improve grid integration metrics compared to the no-storage baseline. The proposed method offers the best grid integration performance with 71% self-consumption rate and only 38% grid dependency through predictive, adaptive scheduling.

4.5. Computational performance

The proposed control strategy is implemented on a desktop computer with Intel Core i7-12700 (2.1 GHz) CPU, 16 GB RAM, and Windows 11 operating system. The MILP problem of upper layer is solved using the CBC optimizer [29]. Table 9 demonstrates the computational performance statistics of the proposed method across the complete 12-month simulation period.

The system operates well within real-time constraints: the hourly MILP in the upper layer solves in under 500 ms on average, with modest memory usage, and the lower-layer greedy tracker executes in microseconds, enabling minute-level demand management. For context on reference methods (same platform and dataset), the rule-based and Lyapunov controllers require on average 0.002 ms and 0.8 ms per time step, respectively. A centralized 15-min MILP requires 20.1 s per solve as reported in prior work [4]. The computational advantage is

Table 8
Grid integration metrics.

Metric	No storage	Rule-based	Lyapunov	Proposed
Self-Consumption Rate (%)	53	69	65	71
PV Utilization Rate (%)	53	69	65	69
Grid Dependency (%)	50	40	42	38

Table 9
Computational performance.

Component	Avg. time (ms)	Max time (ms)	Memory (MB)
Upper Layer MPC	478	882	7.1
Lower Layer Greedy	0.002	0.2	0.0
Forecasting (24 h forecast horizon)	18.2	39.5	8.69
Total System	496	922	15.8

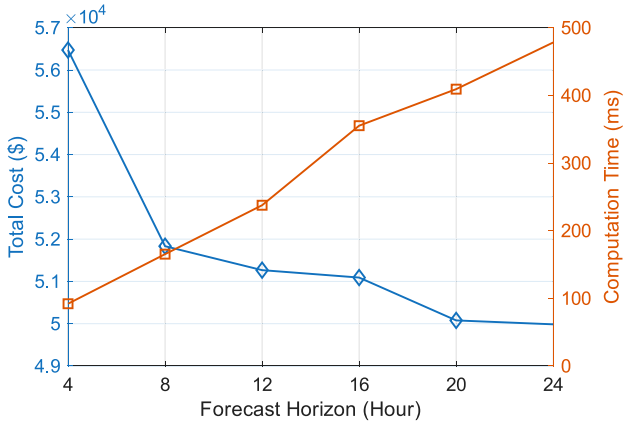

Fig. 8. Total electricity cost and computation time under different forecast horizons.

specifically relative to centralized approaches that attempt simultaneous optimization of energy and demand charges. While rule-based and Lyapunov methods are computationally faster, they sacrifice economic performance; the proposed multi-timescale approach achieves a practical trade-off, delivering near-optimal cost savings within real-time computational limits.

These performance characteristics support deployment on industrial controllers and edge computing platforms commonly used in commercial energy management systems.

4.6. Parameter sensitivity analysis

4.6.1. Forecast horizon impact

Fig. 8 demonstrates the relationship between forecast horizon versus economic performance and computation time. The total cost decreases as forecast horizon increases, but the reduction becomes less significant beyond 8 h. Even with 24-hour forecast horizon, the computation time remains under 500 ms, making it favorable for practical applications.

4.6.2. Threshold parameter impact

The demand charge threshold significantly affects the trade-off between peak reduction and energy arbitrage. Fig. 9 presents the relationship between threshold and electricity cost, demonstrating the critical balance between immediate demand management and long-term energy optimization.

The analysis reveals that both extremely low and high threshold values result in suboptimal performance. Low thresholds drain batteries early, leaving insufficient energy for subsequent peak reduction. High thresholds naturally reduce demand management effectiveness. The optimal threshold balances both objectives and can be selected based on load and PV characteristics. This validates the theoretical framework's emphasis on the threshold as a critical coordination parameter between the two optimization layers. This trade-off highlights the threshold as a critical hyperparameter that should be tuned based on load volatility and PV variability.

The default threshold used in this work is 66 kW, selected as the 95th percentile of historical net grid power observed in 15-minute windows. As seen in Fig. 9, the total cost remains near-optimal over a broad threshold range, demonstrating robustness to threshold variation. Future work may explore adaptive threshold selection strategies, such as using seasonal peak patterns, predictive analytics, or reinforcement learning techniques, to dynamically adjust the threshold for improved long-term performance.

4.6.3. Forecast accuracy impact

The moderate forecasting accuracy has limited impact on overall system performance. A comparison with perfect foresight scenarios in Table 6 reveals only 2.5% cost difference, demonstrating the framework's resilience to forecast errors through two compensating mechanisms. First, the proposed method compensates for forecast uncertainty through feedback [23,30]: the rolling horizon MPC naturally corrects errors by updating optimization hourly based on actual measurements, allowing energy arbitrage planning to adapt to real-time conditions rather than relying solely on predictions. Second, the lower-layer algorithm provides reactive control that immediately adjusts battery dispatch when actual conditions deviate from forecasts and grid power exceeds predefined thresholds. These built-in robustness features effectively mitigate forecast uncertainty while preserving near-optimal economic performance, demonstrating the practical viability of the hierarchical approach without requiring perfect predictions.

4.7. Investment return analysis

The economic viability of the SLBESS deployment is evaluated based on current market conditions and system performance. The investment analysis considers the total capital expenditure (CAPEX) and operational savings achieved through the proposed control strategy.

Based on current market prices for second-life battery systems, the total system cost includes second-life batteries at $100/kWh, balance of system components ranging from $50–150/kWh, and installation and commissioning costs of $50–100/kWh [31–33]. For the 362 kWh/56 kW system studied, the total CAPEX is estimated at $90,500. Annual operation and maintenance costs are approximately 3% of CAPEX [34], resulting in $2715 per year for routine maintenance, monitoring, and component replacement.

The annual electricity cost savings achieved by the proposed method is $20,676. After accounting for annual operation and maintenance (O&M) costs, the net annual savings is $17,961. This results in a simple payback period of 5.0 years and an internal rate of return (IRR) of approximately 14.9% over a 10-year system lifetime considering a 6% discount rate.

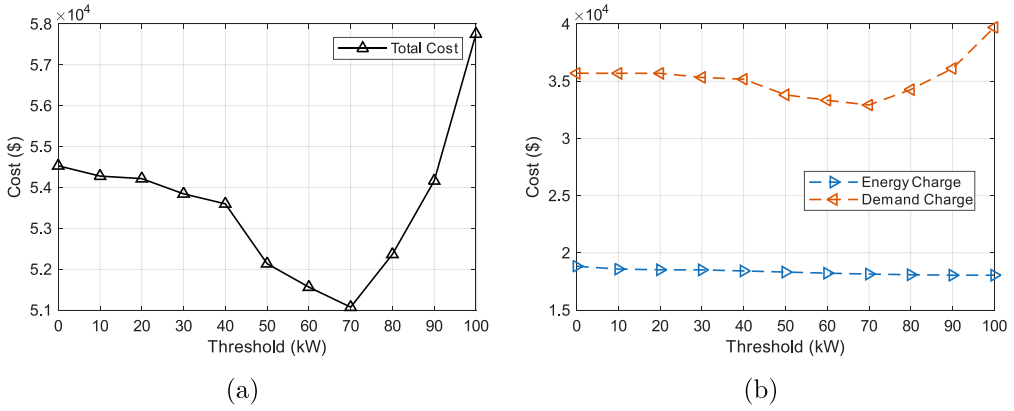

Fig. 9. Electricity cost versus different lower layer threshold values. (a) Total cost. (b) Energy charge and demand charge breakdown.

Compared with the proposed strategy, the rule-based controller yields a slightly longer payback period of 5.5 years, but this comes at the cost of increased battery throughput and accelerated degradation. In contrast, the Lyapunov-based approach yields a substantially longer payback of 10 years, reflecting its lower cost savings and conservative battery usage.

The investment case is further strengthened by several factors. The conservative battery degradation rate of 1.20% annually indicates long operational life, potentially extending beyond the 10-year analysis period. Increasing electricity rates and demand charges will improve future savings, while declining battery replacement costs over the system lifetime enhance long-term economics. These results demonstrate strong financial viability for second-life battery systems in commercial applications when coupled with advanced control strategies.

4.8. Discussion

The experimental validation yields several key insights. The multi-timescale decomposition effectively leverages the temporal structure of electricity pricing, outperforming baseline approaches while maintaining computational efficiency suitable for real-world deployment. Conservative battery operating conditions ensure long-term longevity while still delivering strong economic performance, supporting the business case for second-life battery integration.

Threshold parameter analysis confirms the theoretical framework's emphasis on balancing short-term demand management with long-term energy optimization. Computational results further validate the framework's practicality for real-time commercial applications. Finally, the battery health analysis shows that economic optimization and battery preservation are compatible objectives when appropriate operating constraints are enforced.

The proposed multi-timescale framework is applicable across diverse electricity markets. The hierarchical decomposition exploits the fundamental temporal separation between cumulative energy charges and instantaneous demand charges present in most commercial tariffs worldwide. The upper-layer MPC can be adapted to different energy pricing structures, such as flat rates, real-time pricing, or alternative TOU configurations, by modifying cost coefficients in Eq. (12). The lower-layer algorithm can adjust threshold to adapt to various demand charge mechanisms, such as monthly peaks, seasonal charges, or coincident demand. In markets without separate demand charges, the problem simplifies to a single-layer optimization. Conversely, more complex tariff structures may require further modeling enhancements. Future work should validate this framework across diverse market designs to confirm its generalizability.

The current framework addresses battery aging through conservative operational constraints rather than by explicitly incorporating degradation costs into the optimization objective. Although degradation-aware co-optimization is a more advanced strategy, directly integrating degradation costs would substantially increase computational complexity due to the nonlinear nature of aging models and the need for real-time cycle tracking. For second-life batteries under conservative operation (narrow SOC range, low C-rates), degradation is predictable, and implicit mitigation via operational constraints effectively preserves battery health. The hierarchical architecture supports future integration of cycle-cost terms into the upper-layer objective while maintaining real-time computational tractability in the lower layer.

4.8.1. Limitations and future work

Although this study demonstrates the practical viability of the proposed framework, it is important to acknowledge several limitations and boundary conditions to contextualize the results and inform future research.

(1) Market and tariff dependency: This study focuses on California's TOU tariff, which includes separate energy and demand charges. Although the hierarchical decomposition is broadly applicable to commercial tariffs with temporal separation of energy and demand objectives, the optimal parameters and resulting economic benefits are contingent on the specific pricing structure. Regions with flatter rate structures may yield lower savings than the 28.6% observed in this case.

(2) Forecast accuracy: The XGBoost models achieve moderate accuracy despite the lack of exogenous weather variables. Although the framework exhibits resilience to forecast errors via rolling horizon updates and reactive control, incorporating weather data could enhance PV prediction accuracy, especially in regions with significant weather variability.

(3) Validation period: The field validation spans one month, showing strong agreement between simulation and real-world performance, but it does not capture full seasonal variability. While the 12-month simulation covers annual cycles, extended multi-seasonal field trials are necessary to validate system performance under varied conditions and account for long-term battery aging effects.

(4) Battery aging modeling: The framework employs empirically validated operational constraints (15%–85% SOC, 0.25C limits) instead of explicitly modeling degradation dynamics within the optimization. This strategy offers computational efficiency and is suitable for second-life batteries operated conservatively, where degradation is relatively predictable. The reported 1.20% annual degradation rate is specific to actively controlled battery packs under defined operating conditions. Advanced approaches including data-driven estimation [35], mechanism-based learning [36], and digital twin models [37,38] offer detailed predictions. Future work could integrate simplified versions of these models to enable adaptive operation as battery characteristics evolve.

(5) System scale and configuration: This study validates a specific system size designed for a commercial building with a 0.33 load factor and 200 kW of PV capacity. Buildings with substantially different load profiles or PV-to-load ratios may require customized parameter tuning. The buffer battery configuration leads to uneven aging across battery packs, and the reported metrics reflect only the actively controlled units.
(6) Computational scaling: Although the proposed 24-step MILP solves in under 500 ms on standard hardware, incorporating more complex penalty structures or significantly extending the prediction horizon could increase computational demands. Care must be taken when extending the framework to larger multi-building systems or higher-resolution MPC horizons.

Future research directions shall directly address the limitations identified above. First, extending field validation to multi-seasonal and multi-site deployments will help capture long-term seasonal variability, extreme weather events, and battery aging across diverse operational conditions. Second, integrating degradation-aware co-optimization that explicitly incorporates battery aging costs into the upper-layer MPC objective while maintaining computational tractability will enable adaptive operation as batteries age. This includes developing adaptive parameter estimation techniques to update battery characteristics (such as capacity, resistance, and efficiency) in real-time based on operational data. Third, validating the framework across electricity markets with varying tariff structures (e.g., real-time pricing, capacity markets, ancillary services) will test its generalizability and inform parameter tuning across regulatory contexts. Fourth, integrating weather forecasting into the prediction pipeline will improve PV generation accuracy and enable more proactive energy management. Finally, investigating the framework's scalability to larger commercial buildings, microgrids, and aggregated systems will expand its applicability. These extensions will further improve the framework's performance, adaptability, and deployment potential across diverse commercial energy management scenarios.

5. Conclusion

This paper proposes a multi-timescale control framework for optimizing electricity costs in commercial buildings using second-life battery energy storage systems. The pivotal innovation of this work lies in its temporal decomposition, which directly tackles the computational intractability of centralized optimization under commercial tariff structures. By strategically decoupling the long-term energy arbitrage problem from the short-term peak shaving objective, the framework achieves a critical balance between computational efficiency and economic performance that has been a persistent challenge in the field. This hierarchical design maintained sub-500 ms computation times, making real-time deployment practically feasible while retaining near-optimal economic performance.

A key contribution of this work is comprehensive validation on a deployed SLBESS system using 12 months of real operational data, distinguishing it from predominantly simulation-based studies in the literature. Compared to a no-storage baseline, the framework achieved a 28.6% reduction in electricity costs, outperforming conventional rule-based and Lyapunov-based methods by 6% and 16.1%, respectively. Critically, the framework integrates empirically validated, health-preserving constraints (15%–85% SOC, 0.25C rate limits) that achieve only 1.20% annual battery degradation while maintaining high utilization, demonstrating that economic optimization and battery longevity are compatible objectives under appropriate control strategies. The investment analysis showed a simple payback period of 5.0 years and a 14.9% internal rate of return, supporting the economic feasibility of SLBESS adoption in commercial settings.

The study further confirms several important insights. Threshold parameter sensitivity analysis revealed a robust trade-off space for coordinating long-term energy planning and short-term peak avoidance. Operational metrics demonstrated that economic optimization and battery health preservation can be simultaneously achieved. The framework's resilience to forecast uncertainty, maintaining near-optimal performance despite moderate prediction errors, validates its practical robustness.

Overall, the framework provides a scalable and cost-effective foundation for deploying second-life battery systems in commercial energy management applications. It contributes to reducing electricity costs, improving grid flexibility, and accelerating the circular economy for electric vehicle batteries. Looking forward, future work will directly address the limitations of the current study. This includes: (1) extending field validation to multi-seasonal and multi-site deployments to capture long-term seasonal variability and battery aging effects, (2) integrating degradation-aware co-optimization that explicitly incorporates battery aging costs into the upper-layer MPC objective while maintaining computational tractability, and (3) developing adaptive parameter estimation techniques to update battery characteristics in real-time as the system ages. These extensions will further enhance the framework's performance and generalizability across diverse operational contexts and market structures.

CRediT authorship contribution statement

Zhi Cao: Writing – review & editing, Writing – original draft, Visualization, Validation, Software, Methodology, Investigation, Formal analysis, Data curation, Conceptualization. **Naser Vosoughi Kurdkandi:** Writing – review & editing, Visualization, Conceptualization. **Shengyu Jia:** Writing – review & editing, Validation. **Chris Mi:** Writing – review & editing, Supervision, Resources, Project administration, Funding acquisition.

Declaration of competing interest

The authors declare the following financial interests/personal relationships which may be considered as potential competing interests: Chris Mi reports financial support was provided by California Energy Commission. If there are other authors, they declare that they have no known competing financial interests or personal relationships that could have appeared to influence the work reported in this paper.

Acknowledgments

The authors would like to acknowledge the financial support of the California Energy Commission under grant number EPC-19-053.

Appendix. Multi-timescale cost optimization algorithm

The complete implementation algorithm for the proposed hierarchical control framework is detailed below.

Algorithm 1 Multi-timescale Cost Optimization Algorithm

Initialize: $t = 0$, SOC_0, forecast models, pricing data
while $t < T_{\text{final}}$ **do**
  if $t \bmod 60 = 0$ **then**
    Generate 24-hour load/PV forecasts using XGBoost models
    Update $SOC^k = \text{SOC}_{\text{current}}$ from lower layer actual state
    Solve upper-layer MILP problem Eq. (21)
    Store hourly references $P_{\text{bat}}^{h,*}$ for $h \in [k, k+23]$
  end if
  Execute lower-layer Algorithm in Fig. 3
  Implement control action $P_{\text{bat}}^{*}(t)$
  Update battery SOC and advance time: $t = t + 1$
end while

Data availability

Data will be made available on request.

References

[1] Neigum K, Wang Z. Technology, economic, and environmental analysis of second-life batteries as stationary energy storage: A review. J Energy Storage 2024;103:114393. http://dx.doi.org/10.1016/j.est.2024.114393.

[2] Aguilar Lopez F, Lauinger D, Vuille F, Müller DB. On the potential of vehicle-to-grid and second-life batteries to provide energy and material security. Nat Commun 2024;15(1):4179. http://dx.doi.org/10.1038/s41467-024-48554-0.

[3] Leadbetter J, Swan L. Battery storage system for residential electricity peak demand shaving. Energy Build 2012;55:685–92. http://dx.doi.org/10.1016/j.enbuild.2012.09.035.

[4] Shi J, Ye Z, Gao HO, Yu N. Lyapunov optimization in online battery energy storage system control for commercial buildings. IEEE Trans Smart Grid 2023;14(1):328–40. http://dx.doi.org/10.1109/TSG.2022.3197959.

[5] Jones M, Peet MM. Solving dynamic programming with supremum terms in the objective and application to optimal battery scheduling for electricity consumers subject to demand charges. 2017, http://dx.doi.org/10.48550/arXiv.1708.03714, arXiv:1708.03714.

[6] Jiang Z, Risbeck MJ, Ramamurti V, Murugesan S, Amores J, Zhang C, et al. Building HVAC control with reinforcement learning for reduction of energy cost and demand charge. Energy Build 2021;239:110833. http://dx.doi.org/10.1016/j.enbuild.2021.110833.

[7] Lee J-H, Park J-Y, Sim H-S, Lee H-S. Multi-residential energy scheduling under time-of-use and demand charge tariffs with federated reinforcement learning. IEEE Trans Smart Grid 2023;14(6):4360–72. http://dx.doi.org/10.1109/TSG.2023.3251956.

[8] Kumar R, Wenzel MJ, Ellis MJ, ElBsat MN, Drees KH, Zavala VM. A stochastic model predictive control framework for stationary battery systems. IEEE Trans Power Syst 2018;33(4):4397–406. http://dx.doi.org/10.1109/TPWRS.2017.2789118.

[9] Jahid Hasan ASM, Yusuf J, Rahman MS, Islam MS. Electricity cost optimization for large loads through energy storage and renewable energy. In: 2023 international conference on information and communication technology for sustainable development. 2023, p. 46–50. http://dx.doi.org/10.1109/ICICT4SD59951.2023.10303409.

[10] Zhou HS, Passey R, Bruce A, Sproul AB. Aggregated impact of coordinated commercial-scale battery energy storage systems on network peak demand, and financial outcomes. Renew Sustain Energy Rev 2021;144:111014. http://dx.doi.org/10.1016/j.rser.2021.111014.

[11] Hasan ASMJ, Enriquez-Contreras LF, Yusuf J, Ula S. A comprehensive building load optimization method from utility rate structure perspective with renewables and energy storage. In: 2021 international conference on smart energy systems and technologies. 2021, p. 1–6. http://dx.doi.org/10.1109/SEST50973.2021.9543188.

[12] Ju C, Wang P, Goel L, Xu Y. A two-layer energy management system for microgrids with hybrid energy storage considering degradation costs. IEEE Trans Smart Grid 2018;9(6):6047–57. http://dx.doi.org/10.1109/tsg.2017.2703126

[13] Pan C, Fan H, Zhang R, Sun J, Wang Y, Sun Y. An improved multi-timescale coordinated control strategy for an integrated energy system with a hybrid energy storage system. Appl Energy 2023;343:121137. http://dx.doi.org/10.1016/j.apenergy.2023.121137.

[14] Guo X, Che Y, Zheng Z, Sun J. Multi-timescale optimization scheduling of interconnected data centers based on model predictive control. Front Energy 2024;18(1):28–41. http://dx.doi.org/10.1007/s11708-023-0912-6.

[15] Zafar R, Ravishankar J, Fletcher JE, Pota HR. Multi-timescale model predictive control of battery energy storage system using conic relaxation in smart distribution grids. IEEE Trans Power Syst 2018;33(6):7152–61. http://dx.doi.org/10.1109/TPWRS.2018.2847400.

[16] Jung S-W, An Y-Y, Suh B, Park Y, Kim J, Kim K-I. Multi-agent deep reinforcement learning for scheduling of energy storage system in microgrids. Mathematics 2025;13(12):1999. http://dx.doi.org/10.3390/math13121999.

[17] Liu D, Zhong S, Wu L, Zou Y, Tang C. Hierarchical energy management and real-time optimization strategy for household based on multi-agent reinforcement learning. Sustain Energy, Grids Networks 2025;43:101785. http://dx.doi.org/10.1016/j.segan.2025.101785.

[18] Ali MA, Besheer AH, Emara HM, Bahgat A. Optimal micro-grid battery scheduling within a comprehensive smart pricing scheme. Sci Rep 2025;15(1):20098. http://dx.doi.org/10.1038/s41598-025-02690-9.

[19] Alam MM, Rahman MH, Ahmed MF, Chowdhury MZ, Jang YM. Deep learning based optimal energy management for photovoltaic and battery energy storage integrated home micro-grid system. Sci Rep 2022;12(1):15133. http://dx.doi.org/10.1038/s41598-022-19147-y.

[20] Hossain J, Saeed N, Manojkumar R, Marzband M, Sedraoui K, Al-Turki Y. Optimal peak-shaving for dynamic demand response in smart Malaysian commercial buildings utilizing an efficient PV-BES system. Sustain Cities Soc 2024;101:105107. http://dx.doi.org/10.1016/j.scs.2023.105107.

[21] Gao W, Cao Z, Fu Y, Turchiano C, Kurdkandi NV, Gu J, et al. Comprehensive study of the aging knee and second-life potential of the nissan leaf e+ batteries. J Power Sources 2024;613:234884. http://dx.doi.org/10.1016/j.jpowsour.2024.234884.

[22] Gao W, Cao Z, Kurdkandi NV, Fu Y, Mi C. Evaluation of the second-life potential of the first-generation nissan leaf battery packs in energy storage systems. ETransportation 2024;20:100313. http://dx.doi.org/10.1016/j.etran.2024.100313.

[23] Zhang Y, Wang R, Zhang T, Liu Y, Guo B. Model predictive control-based operation management for a residential microgrid with considering forecast uncertainties and demand response strategies. IET Gener Transm Distrib 2016;10(10):2367–78. http://dx.doi.org/10.1049/iet-gtd.2015.1127.

[24] Chen T, Guestrin C. XGBoost: A scalable tree boosting system. In: Proceedings of the 22nd ACM SIGKDD international conference on knowledge discovery and data mining. New York, NY, USA: Association for Computing Machinery; 2016, p. 785–94. http://dx.doi.org/10.1145/2939672.2939785.

[25] Zhang T, Zhang X, Rubasinghe O, Liu Y, Chow YH, Iu HHC, et al. Long-term energy and peak power demand forecasting based on sequential-XGBoost. IEEE Trans Power Syst 2024;39(2):3088–104. http://dx.doi.org/10.1109/TPWRS.2023.3289400.

[26] Qin J, Chow Y, Yang J, Rajagopal R. Online modified greedy algorithm for storage control under uncertainty. IEEE Trans Power Syst 2016;31(3):1729–43. http://dx.doi.org/10.1109/TPWRS.2015.2440355, arXiv:1405.7789.

[27] ASTM E. 1049-85,"Standard practices for cycle counting in fatigue analysis". Annu Book ASTM Stand 2005;3(01):614–20.

[28] Akpinar KN, Gundogdu B, Ozgonenel O. A novel cycle counting perspective for energy management of grid integrated battery energy storage systems. Energy Rep 2023;9:123–31. http://dx.doi.org/10.1016/j.egyr.2022.10.359.

[29] Forrest J, Ralphs T, Vigerske S, Santos HG, Forrest J, Hafer L, et al. Coin-or/cbc: release releases/2.10.12. 2024, http://dx.doi.org/10.5281/zenodo.13347261, Zenodo.

[30] Zhang J, Sun K, Li C, Yang H, Zhou B, Hou X, et al. MPC-based co-optimization of an integrated PV-EV-Hydrogen station to reduce network loss and meet EV charging demand. eTransportation 2023;15:100209. http://dx.doi.org/10.1016/j.etran.2022.100209.

[31] Nichols C. Second-life electric vehicle batteries 2025–2035: Markets, forecasts, players, and technologies. Tech. rep., Cambridge: IDTechEx; 2024, URL https://www.idtechex.com/en/research-report/second-life-ev-batteries-2025/1056. [Accessed 24 September 2025].

[32] Dong Q, Liang S, Li J, Kim HC, Shen W, Wallington TJ. Cost, energy, and carbon footprint benefits of second-life electric vehicle battery use. iScience 2023;26(7):107195. http://dx.doi.org/10.1016/j.isci.2023.107195.

[33] Cole W, Karmakar A. Cost projections for utility-scale battery storage: 2023 update. Tech. rep., Golden, CO: National Renewable Energy Laboratory; 2023, URL https://www.nrel.gov/docs/fy23osti/85332.pdf. [Accessed 24 September 2025].

[34] ExenCell. BESS costs analysis: Understanding the true costs of battery energy storage systems. 2024, ExenCell Blog. URL https://exencell.com/blogs/bess-costs-analysis-understanding-the-true-costs-of-battery-energy-storage-systems. [Accessed 24 September 2025].

[35] Zhou X, Han X, Wang Y, Lu L, Ouyang M. A data-driven LiFePO4 battery capacity estimation method based on cloud charging data from electric vehicles. Batteries 2023;9(3):181. http://dx.doi.org/10.3390/batteries9030181.

[36] Zhou X, Han X, Shi K, Chen X, Guo D, Zheng Y, et al. Intelligent battery life management through mechanism and machine learning under real vehicle working conditions. J Power Sources 2025;640:236749. http://dx.doi.org/10.1016/j.jpowsour.2025.236749.

[37] Park S, Lee H, Choi S, Lim J, Kim S, Song J, et al. Microstructure-based digital twin thermo-electrochemical modeling of LIBs at the cell-to-module scale. eTransportation 2024;22:100370. http://dx.doi.org/10.1016/j.etran.2024.100370.

[38] Gupta N, Ge S, Sasaki T, Qin K, Longchamps RS, Aotani K, et al. Simulation of single-layer internal short circuit in anode-free batteries. eTransportation 2024;22:100380. http://dx.doi.org/10.1016/j.etran.2024.100380.